Available online at www.sciencedirect.com
ScienceDirect
Journal of Power Sources 170 (2007) 235–241
JOURNAL OF POWER SOURCES
www.elsevier.com/locate/jpowsour

Transient evolution of carbon monoxide poisoning effect of PBI membrane fuel cells

Chien-Ping Wang [a,1], Hsin-Sen Chu [a,*], Yi-Yie Yan [b], Kan-Lin Hsueh [b]

[a] *Department of Mechanical Engineering, National Chiao Tung University, Hsinchu 300, Taiwan, ROC*
[b] *Energy and Environment Laboratories, Industrial Technology Research Institute, Hsinchu 310, Taiwan, ROC*

Received 13 February 2007; received in revised form 19 March 2007; accepted 29 March 2007
Available online 18 April 2007

Abstract

High temperature polybenzimidazole membrane fuel cells are the focus of attention due to high CO tolerance and overcoming water managements. This paper develops a transient, one-dimensional mathematical model to predict CO tolerance, and validates it with experiments. Experimental results are measured at different temperatures. Fuel cell performance degradations with time are also measured under various fuel compositions. Transient evolutions of current density, H_2 coverage, CO coverage, and ionic potential are shown during the CO poisoning process. The theoretical results show that hydrogen coverage decreases with time, reducing hydrogen oxidation reactions and dropping ionic potential loss. The effects of temperature, CO contents, and H_2 dilutions on fuel cell performance and the time to reach steady t_{ss} are all investigated. Predictions of fuel cell current density degradation also show good agreement with experimental results.

Keywords: PBI membrane; PEM fuel cell; Transient evolution; CO poisoning

1. Introduction

Proton exchange membrane fuel cells as alternative power sources are gaining considerable attention due to high energy density and their pollution free environment potential. Pure hydrogen can produce PEMFC highest performance, but is not a proper option due to hydrogen storage and production difficulties. PEM fuel cells working at low temperature encounter major problems such as low CO tolerance and water management. Preferential oxidation and water–gas-sift reaction are usually adopted to bring CO content down to an infinitesimal level. High temperature polybenzimidazole (PBI) membrane fuel cells are receiving recent attention. Wainright et al. [1] applied an acid-doped PBI membrane for fuel cells. PBI is a basic polymer and exhibits high conductivity through doping with various acids or bases. Sulphuric acid and phosphoric acid are the most widely used doping matter to perform high membrane conductivity. Li et al. [2] investigates the dependence of electrical conductivity on acid doping level of phosphoric acid-doped PBI membrane fuel cell. Acid doping level, water uptake, water drag coefficient and mechanical strength are all investigated. Proton conductivity of PBI and PBI composite membrane is influenced by temperature, acid doping level and humidity [3]. Li et al. [4] studies the influence of doping level and water uptake of PBI membrane fuel cells. Methanol permeation and proton conductivity of poly(*N*-ethylbenzimidazole) (PNEBI), poly(*N*-methylbenzimidazole) (PNMBI) and PBI are investigated by Pu et al. [5]. Ma et al. [6] establishes a complete set of membrane conductivity under various RHs, temperatures and acid doping levels.

The operating temperature of acid-doped PBI membrane fuel cells is much higher than PFSA polymer membrane fuel cells. Several advantages make it superior to low temperature PEMFC. Firstly, operating temperature up to 200 °C can tolerate up to 3% CO in anode hydrogen fuel [7]. Dhar et al. [8,9] indicates that CO adsorption at platinum catalysts occurs easily at low temperature. Thus, PBI membrane makes it possible to feed reformed gas directly into the fuel cell at elevated temperature and simplifies the fuel cell system. Secondly, water management such as liquid water flooding and membrane dehydration can be neglected at elevated temperatures higher than the boiling point

* Corresponding author. Tel.: +886 3 5712171x55141; fax: +886 3 5727930.
E-mail address: hschu@cc.nctu.edu.tw (H.-S. Chu).
[1] Graduate student.

0378-7753/$ – see front matter © 2007 Elsevier B.V. All rights reserved.
doi:10.1016/j.jpowsour.2007.03.070

Nomenclature

a	contact area of Pt catalyst ($cm^2\ cm^{-3}$)
C	concentration of reactant gas ($mol\ cm^{-3}$)
D	diffusion coefficient ($cm^2\ s^{-1}$)
i	current density ($A\ cm^{-2}$)
k	conductivity of the Nafion phase
k_{eH}	hydrogen electro-oxidation rate constant ($A\ cm^{-2}$)
k_{eCO}	CO electro-oxidation rate constant ($A\ cm^{-2}$)
n	number of electrons
P	total pressure (atm)
R	universal gas constant ($J\ mol^{-1}\ K^{-1}$)
T	temperature (K)
t	time (min)
x	distance (μm)

Superscripts

in	inlet at catalyst layer

Subscripts

CO	carbon monoxide
CL	catalyst layer
H_2	hydrogen
MEM	membrane
O_2	oxygen
ss	steady state

Greek

ε	porosity
θ	coverage ratio on Pt catalyst site
ϕ	ionic potential (V)
ϕ_s	phase potential of solid phase of electrode (V)
$\delta(\Delta E_H)$	activation energy change for hydrogen dissociative adsorption near CO occupied sites ($J\ mol^{-1}$)
$\delta(\Delta G_{CO})$	variation of free energy of CO adsorption between zero and full coverage ($J\ mol^{-1}$)

of liquid water. He et al. [3] indicates that relative humidity has less influence on PBI membrane conductivity than the Nafion membrane. Fuel cells working at high temperature can convert into a compact design with methanol reformer [10,11]. This is because nearly 100% conversion is made around 200 °C through methanol steam reforming [11]. Reformed gas not only feeds directly into the fuel cell, but also provides a sufficient amount of heat for fuel cells.

Several experiments analyze high temperature PBI membrane fuel cells, but only a few theoretical studies are available. Cheddie and Munroe [12] apply a one-dimensional model to predict PBI membrane fuel cell performance. Korsgaard et al. [13] use a semi empirical model to approach the experimental data of PBI membrane fuel cell polarization curves. However, theoretical investigations examining the fundamental transportation inside PBI membrane fuel cells are still lacking. Qualitative experiments are needed to optimize fuel cell system designs. This paper investigates PBI membrane fuel cell performance under various fuel compositions from both simulation and experiments, including effects of temperature, CO content, and hydrogen concentration on cell performance and t_{ss}. The transportations of hydrogen coverage, CO coverage on platinum catalysts, and ionic potential loss across the MEA are shown in the simulation results.

2. Experiments

The experiments use a five-layered membrane electrode assembly with PBI membrane, Pt catalyst, and carbon papers. Total thickness of the MEA is 971 μm and a 45.2 cm^2 active area. The end plates were made by aluminum alloy with isolated treatment to give rigid support. The serpentine flow channels were manufactured on graphite plates with 1 mm × 1 mm channel sizes.

Inlet gases are supplied via model PC-540 mass flow controller (Protec Instruments, Inc.). High power electronic load model 3316-04 is made by Prodigit Electronics Co., Ltd. The ITRI test station measures polarization curves and other experimental results. Fuel cells are operated without gas humidification, resulting in simpler operation processes and avoiding water management problems, such as flooding. Fuel cell operating temperature is around 120–180 °C through YSC (GX-36) temperature controllers to maintain desired operating temperature. Temperature below water boiling temperature can cause phosphoric acid dissolution in liquid water and drop membrane conductivity. The time required for MEA activation is generally 30–50 h at a given constant current density ($0.2\ A\ cm^{-2}$) with a maximum stoichiometric of $\lambda = 2.5$ during start-up for both the anode and cathode side.

Fuel cell testing is performed under various gas mixtures, 1–3% CO, 40–55% H_2, 20% CO_2, balanced with N_2. Pure hydrogen and air are applied to anode and cathode, respectively until fuel cell reaches steady state. Then, a CO mixed stream replaces pure hydrogen.

3. Theoretical model

A three layer mathematical model developed in this work analyzes the transient CO poisoning process of high temperature PBI membrane fuel cells. An MEA schematic model is shown in Fig. 1, representing the anode catalyst layer, membrane, and cathode catalyst layer. Table 1 represents all the governing equations. Gas species transport at the catalyst layers is described as

$$N_i = -D_i \varepsilon_{CL}^{1.5} \nabla C_i \quad (1)$$

where N_i represents flux of gas species including hydrogen, oxygen, and carbon monoxide, ε_{CL} the porosity at both the anode and the cathode catalyst layer and C_i expresses concentration of gases. Protons are produced from hydrogen oxidation reactions at the anode catalyst layer and then transport toward the fuel cell cathode through the membrane. Current density at the membrane can be expressed as:

$$i = -k_n \nabla \phi \quad (2)$$

Table 1
Governing equations

Variables	ACL	MEM	CCL
C_{H_2}	$\frac{\partial}{\partial t}[\varepsilon_{CL} C_{H_2}] = -\nabla \cdot N_{H_2} - R_{H_2}$	$C_{H_2} = 0$	$C_{H_2} = 0$
C_{O_2}	$C_{O_2} = 0$	$C_{O_2} = 0$	$\frac{\partial}{\partial t}[\varepsilon_{CL} C_{O_2}] = -\nabla \cdot N_{O_2} - R_{O_2}$
C_{CO}	$\frac{\partial}{\partial t}[\varepsilon_{CL} C_{CO}] = -\nabla \cdot N_{CO} - R_{CO}$	$C_{CO} = 0$	$C_{CO} = 0$
ϕ	$k_{eff}\nabla^2\phi - (R_{H_2} + R_{CO}) = 0$	$k_n \nabla^2 \phi = 0$	$k_{eff}\nabla^2\phi - R_{O_2} = 0$

in which k_n is the membrane conductivity and ϕ is the electrolytic phase potential [14]. Water inside the fuel cell can be treated as a vapor phase because PBI membrane fuel cells work higher than 120 °C. Thus, the represented hydrogen and carbon monoxide current densities can be reduced from [15]:

$$\frac{di_{H_2}}{dx} = 2ak_{eH}\theta_{H_2} \sinh\left(\frac{n_{H_2}F(\phi_s - \phi - U_0)}{2RT}\right) \quad (3)$$

$$\frac{di_{CO}}{dx} = 2ak_{eCO}\theta_{CO} \sinh\left(\frac{n_{CO}F(\phi_s - \phi - U_0)}{2RT}\right) \quad (4)$$

where k_{eH} and k_{eCO} are the rate constants of hydrogen and CO electro-oxidation [16,17], ϕ_s and U_0 represent phase potential of solid phase of electrode and thermodynamic equilibrium potential, respectively. The calculations of unsteady state θ_{H_2} and θ_{CO} can be referred to [15]. The forward rate constant of hydrogen k_{fH} and CO adsorption-to-desorption rate ratios b_{fC} are expressed as:

$$k_{fh} = k_{fH0} \cdot \exp\left[-\frac{\delta(\Delta E_H)}{RT}\left(1 - \exp\left(\frac{\lambda\theta_{CO}}{\theta_{CO} - 1}\right)\right)\right] \quad (5)$$

$$b_{fCO} = b_{fCO0} \cdot \exp\left[\frac{\delta(\Delta G_{CO})}{RT}\theta_{CO}\right] \quad (6)$$

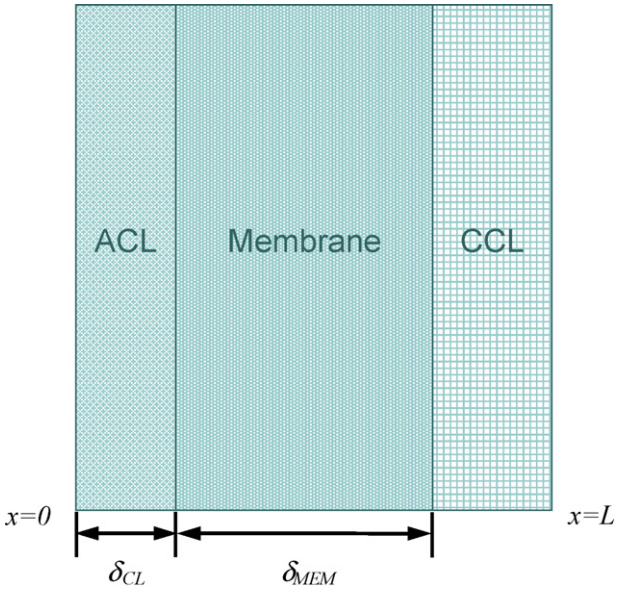

Fig. 1. An MEA schematic model.

The reaction rates of hydrogen and carbon monoxide are expressed as:

$$R_{H_2} = \frac{di_{H_2}}{dz}\left(\frac{\gamma_{H_2}}{n_{H_2}F}\right) \quad (7)$$

$$R_{CO} = \frac{di_{CO}}{dz}\left(\frac{\gamma_{CO}}{n_{CO}F}\right) \quad (8)$$

where γ and n represent stoichiometric ratio and number of electrons, respectively. Oxygen reaction rate at the cathode catalyst layer is given by [15]:

$$R_{O_2} = \frac{1}{4F}(1 - \bar{\theta}_{CO})ai_0\left[\frac{C_{O_2}}{C_{O_{2ref}}}\exp\left(\frac{-F(\phi_s - \phi - U_0)}{RT}\right)\right] \quad (9)$$

in which $\bar{\theta}_{CO}$ is the average value of CO coverage calculated from the anode. Table 2 lists the corresponding boundary conditions applied in the numerical computation. Table 3 shows the parameters used in this paper. The steady-state condition is defined as the relative error of current density reaches:

$$\frac{i^{n+1} - i^n}{i^n} \le 10^{-3} \quad (10)$$

in which i^n represents current density at nth min.

Table 2
Boundary conditions

Variables	$x = 0$	ACL/MEM	MEM/CCL	$x = L$
C_{H_2}	$C_{H_2} = C^{in}_{H_2}$	$N_{H_2} = 0$	N/A	N/A
C_{O_2}	N/A	N/A	$N_{O_2} = 0$	$C_{O_2} = C^{in}_{O_2}$
C_{CO}	$C_{CO} = C^{in}_{CO}$	$N_{CO} = 0$	N/A	N/A
ϕ	$\phi = 0$	$k_{n,eff}\nabla\phi = k_n\nabla\phi$	$k_{n,eff}\nabla\phi = k_n\nabla\phi$	$\nabla\phi = 0$

Table 3
The parameters used in the present theoretical model

Temperature (T)	453 K
Total pressure (P)	1 atm
Diffusion coefficient of hydrogen in gas phase (D_{H_2})	1.1028 ($cm^2\ s^{-1}$)
Diffusion coefficient of oxygen in gas phase (D_{O_2})	$0.1775 \times (T/273.15)^{1.823}$ ($cm^2\ s^{-1}$)
Thickness of catalyst layer (δ_{CL})	20 (μm)
Thickness of membrane (δ_{MEM})	30 (μm)
Gas porosity in catalyst layer (ε_{CL})	0.4
Ionic conductivity (k_n)	0.09 (mho cm^{-1})

4. Results and discussion

Higher temperature fuel cells are expected to have higher CO tolerance because faster chemical kinetics facilitate CO desorption on the Pt catalyst. Further advantages such as without water–gas-shift reaction, preferential oxidation, and water management can obviously simplify the fuel cell system and lower cost. Theoretical and experimental studies both investigated the transportation of phosphoric acid-doped PBI membrane fuel cells. Fig. 2 shows the transient evolution of hydrogen coverage in the anode catalyst layer with time under 55% H_2 containing 1% CO. Fuel cell operates without carbon monoxide poisoning when time equals zero. Hydrogen currently occupies the highest reaction surface on platinum catalysts, gradually decreasing with time. Strong chemical bonding favors CO adsorption on the Pt catalyst. At $t = 0$, hydrogen coverage decreases from 0.52 to 0.37 at steady state. Thus, cell performance decreases with decreasing hydrogen coverage. Fig. 3 shows opposite trends and depicts CO coverage across the anode catalyst layer. CO coverage is initially at zero and reaches 0.29 until steady state.

Fig. 4 depicts variations of ionic potential profiles across MEA with time. Linear ionic potential profiles are shown since constant ionic conductivity is assumed and protons are not consumed across the membrane. Ionic potential shows nonlinear profiles in the cathode catalyst layer due to oxidant consumption by reduction reactions. Ionic potential loss decreases with time during the CO poisoning process, lowering cell current density. Fig. 5 represents the distribution of θ_{H_2} under various hydrogen dilutions with 1% CO in the anode catalyst layer. At 40% hydrogen, θ_{H_2} has the lowest value and obviously increases with hydrogen content. A larger amount of hydrogen can cover more catalyst reaction surfaces. Increased hydrogen content at higher hydrogen dilution can increase a greater amount of hydrogen coverage than at lower hydrogen dilution. CO coverage under various hydrogen contents reveals opposite trends shown in Fig. 6. At lower hydrogen content, CO has more opportunity to cover Pt catalysts. Hydrogen dilution by comparison, has much more significant effect on θ_{H_2} than on θ_{CO}-inlet fuel containing CO can decrease cell performance with time. Fig. 7 illustrates time to reach steady state t_{ss} under different fuel compositions. CO concentration amounts range from 0.1 to 3% with 40 to 80% hydrogen content. The figure shows that t_{ss} dramatically decreases with increased CO content. High CO concentrations greater than 1% show a much smaller drop rate of t_{ss}. Different hydrogen contents show similar trends. Inlet fuel containing more than 1% CO shows only slight difference in time to reach steady state. Hydrogen dilution effect at low CO concentrations does not show significant difference on time t_{ss}, but gradually increases with CO amount. Increasing hydrogen amount,

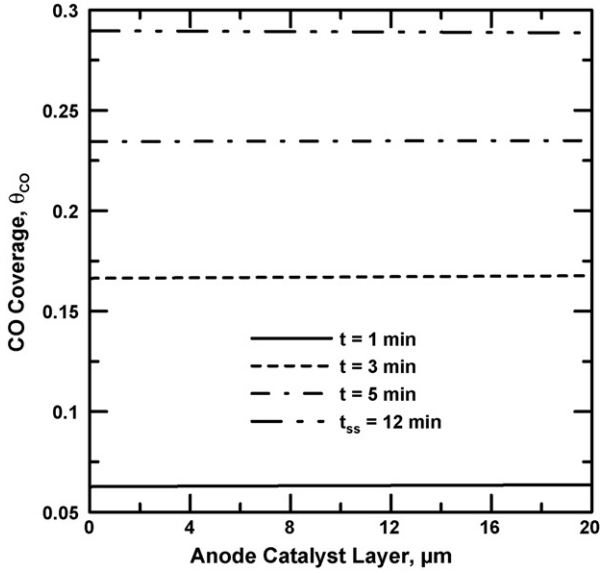

Fig. 3. Transient evolution of CO coverage profiles in anode catalyst layer under 55% H_2 containing 1% CO at 0.6 V.

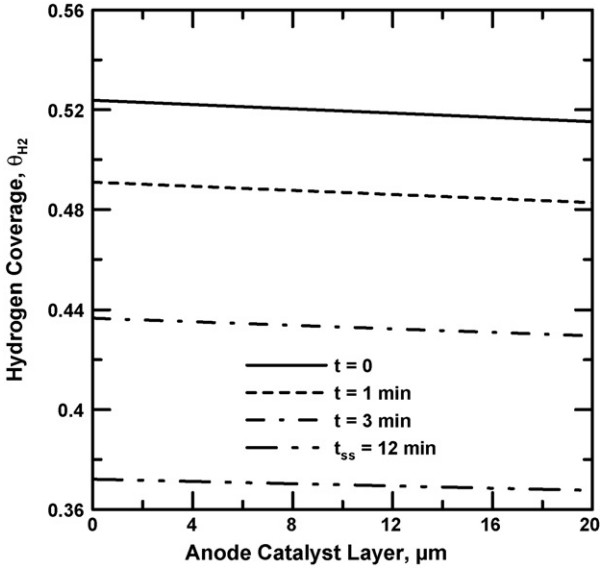

Fig. 2. Transient evolution of hydrogen coverage profiles in the anode catalyst layer under 55% H_2 containing 1% CO at 0.6 V.

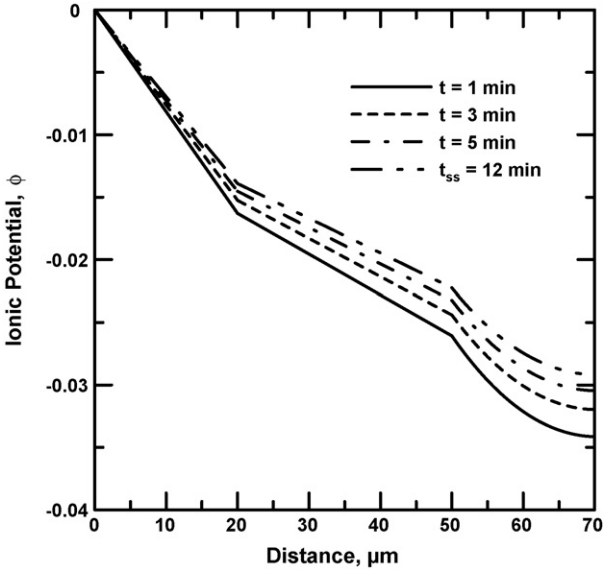

Fig. 4. The distributions of ionic potential loss across MEA with time under 55% H_2 containing 1% CO at 0.6 V.

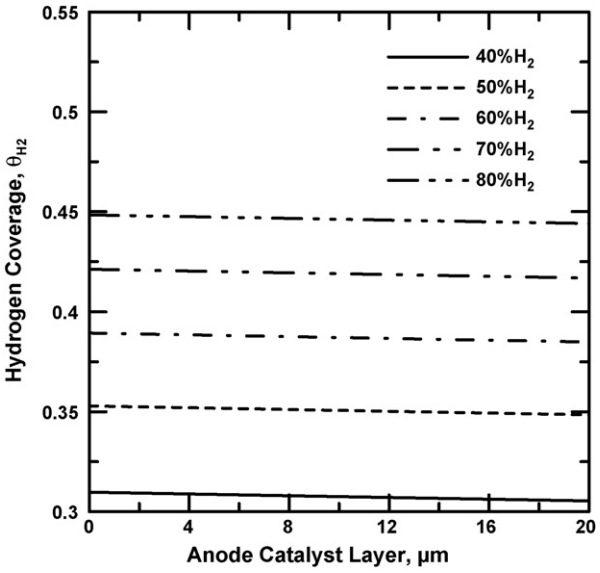

Fig. 5. Hydrogen coverage profiles across the anode catalyst layer under various hydrogen contents with 1% CO at 0.6 V.

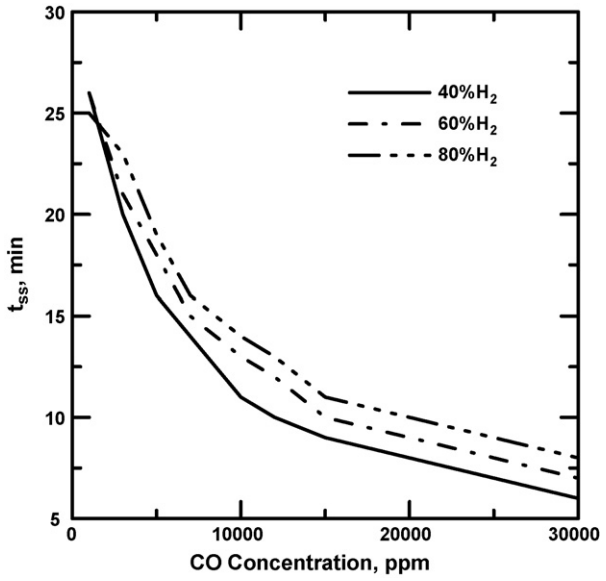

Fig. 7. Effects of CO contents on the time to reach steady state under various hydrogen dilutions at 0.6 V.

especially at higher CO concentrations, can obviously increase the time t_{ss}. Greater amount of hydrogen facilitates hydrogen adsorption on the platinum catalysts.

Fig. 8 plots CO and hydrogen concentration influence on cell current density. Theoretical results show that increased CO concentrations from 0.1 to 3% can dramatically drop cell current density due to greater CO adsorption on Pt catalysts. Also, CO desorption does not easily occur due to strong chemical bonding between CO and Pt, thus accumulating on the catalysts. Increased hydrogen content does not cause significant fuel cell performance improvement with 0.1% CO. However, hydrogen dilution effect becomes much more significant with increasing CO concentration. At 3% CO, a significant increase of fuel cell current density is obtained with increasing hydrogen content from 40 to 80%. Similar hydrogen dilution trends are also shown on time t_{ss}. Fig. 9 shows percentage of energy loss of fuel cell power density under various fuel compositions. A wide range of fuel compositions, including CO and hydrogen content, are considered as important design parameters of methanol reformers. This figure allows for easy reformer specification and convenient performance prediction of designing fuel cells.

Experimental measurements of PBI membrane fuel cell polarization curves at temperature 120, 140, 160 and 180 °C are depicted in Fig. 10. Experiments were all conducted under atmospheric pressure. Fuel and oxidant were fed into the cell directly without extra humidification. The measurements were performed at a stoichiometry ratio of 2.0 of the anode and cathode. Fuel and oxidant were applied with pure hydrogen and

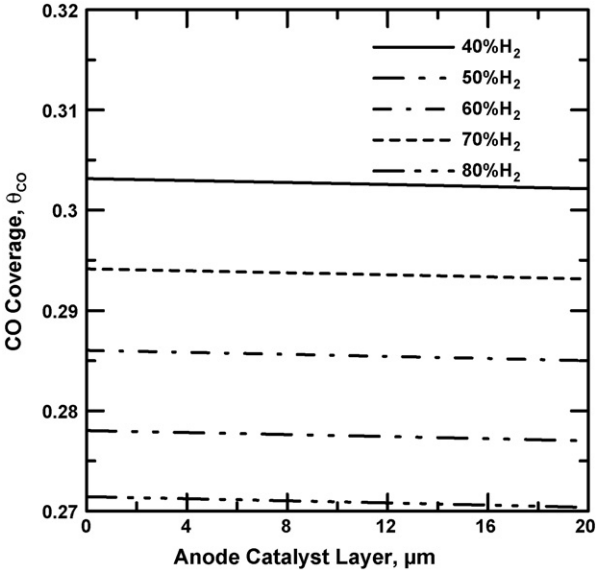

Fig. 6. CO coverage profiles across the anode catalyst layer under various hydrogen contents with 1% CO at 0.6 V.

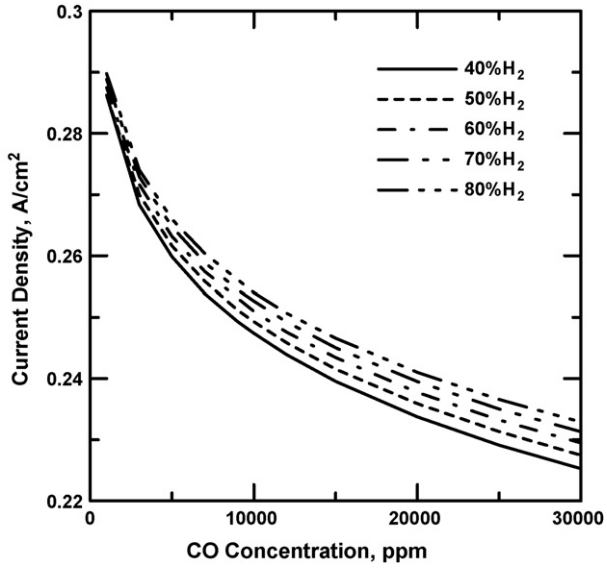

Fig. 8. Effects of CO contents on current density under various hydrogen concentrations at 0.6 V.

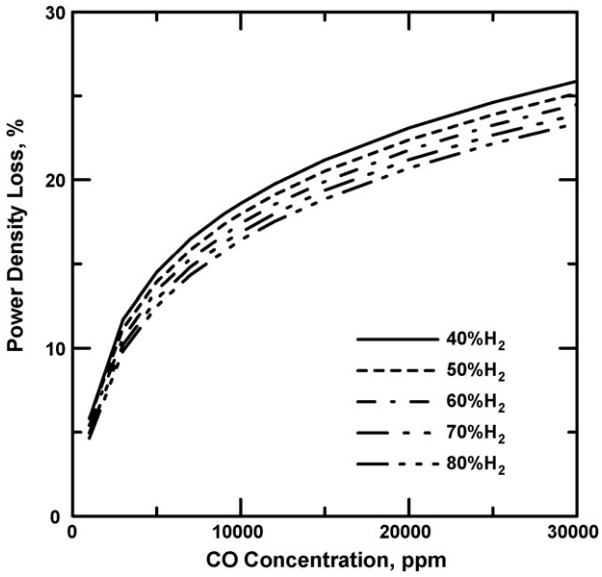

Fig. 9. Percentage of power density loss under various fuel compositions at 0.6 V.

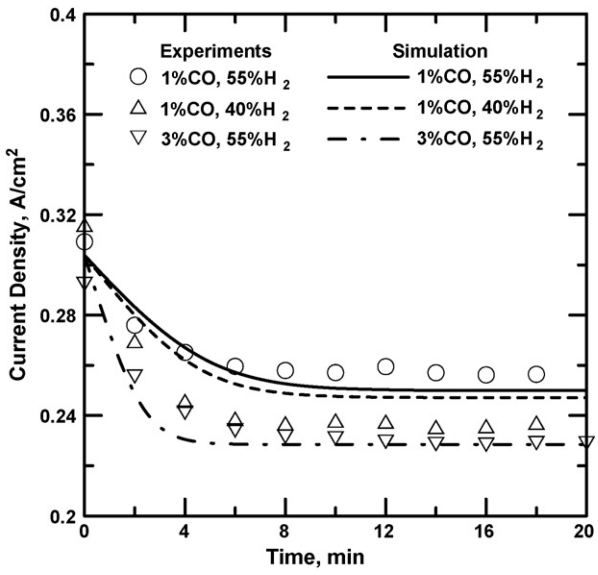

Fig. 11. Simulation result comparisons with experimental data at 0.6 V.

air, respectively. Highest performance is seen at temperature 180 °C and significantly decreases with temperature drop. This is because membrane conductivity increases at higher temperature. Electrode kinetics also becomes faster at higher temperature. Membrane dehydration is not shown at elevated temperature of PBI membrane fuel cell. Fig. 11 plots simulation result comparisons with experimental data. Fuel cell performance degradation with time is shown under various fuel compositions containing 1–3% CO and 40–55% H_2. Transient evolutions of cell performance are accurately predicted from simulations and also measured by experiments. Current density drops with time and reaches steady state in a few minutes. Good agreements are plotted in this figure. The difference between simulation and experiments is relative large for the case with 1% CO and 40% H_2. Following assumptions may cause this discrepancy. First, hydrogen and CO coverage are assumed to be linear relation with current density distribution. Second, flow channel and gas diffusion layer are neglected in the theoretical model. This may influences the transport of fuel and oxidant. Results also show the effects of hydrogen dilution and CO concentration on current density and time t_{ss}.

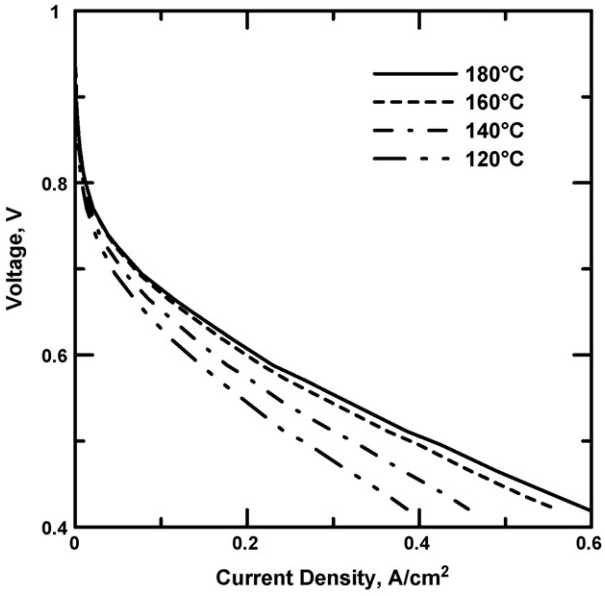

Fig. 10. Experimental measurements of PBI membrane fuel cell polarization curves at temperature 120, 140, 160 and 180 °C at 0.6 V.

5. Conclusions

The present study develops a transient, one-dimensional mathematical model to analyze PBI membrane fuel cells. Various fuel compositions are considered to realize the effect of fuel composition such as CO concentration and hydrogen dilution of the fuel cell. Chemical bonding is much stronger between CO and the Pt catalyst than hydrogen; therefore CO easily accumulates on the catalyst. Thus, hydrogen coverage rapidly declines with time. Higher CO content and hydrogen dilution also cause significant increase on CO coverage. Ionic potential loss decreases with time during the CO poisoning process. Simulation results show good agreement with experimental data. The simulation from this work can accurately predict fuel cell performance under various fuel compositions and realize transient degradations of fuel cell performance, thus providing sufficient information for the designing reformer and fuel cell system.

References

[1] J.S. Wainright, J.-T. Wang, R.F. Savinell, M. Litt, J. Electrochem. Soc. 142 (1995) L121.
[2] Q. Li, H.A. Hjuler, N.J. Bjerrum, J. Appl. Electrochem. 31 (2001) 773.
[3] R. He, Q. Li, G. Xiao, N.J. Bjerrum, J. Membr. Sci. 226 (2003) 169.
[4] Q. Li, R. He, R.W. Berg, H.A. Hjuler, N.J. Bjerrum, Solid State Ionics 168 (2004) 177.

[5] H. Pu, Q. Liu, G. Liu, J. Membr. Sci. 241 (2004) 169.
[6] Y.-L. Ma, J.S. Wainright, M.H. Litt, R.F. Savinell, J. Electrochem. Soc. 151 (2004) A8.
[7] Q. Li, R. He, J. Gao, J.O. Jensen, N.J. Bjerrum, Solid State Ionics 150 (2003) 1599.
[8] H.P. Dhar, L.G. Christner, A.K. Kush, H.C. Maru, J. Electrochem. Soc. 133 (1986) 1574.
[9] H.P. Dhar, L.G. Christner, A.K. Kush, J. Electrochem. Soc. 134 (1987) 3021.
[10] J.D. Holladay, J.S. Wainright, E.O. Jones, S.R. Gano, J. Power Sources 130 (2004) 111.
[11] C. Pan, R. He, Q. Li, J.O. Jensen, N.J. Bjerrum, H.A. Hjulmand, A.B. Jensen, J. Power Sources 145 (2005) 392.
[12] D. Cheddie, N. Munroe, Energy Convers. Manage. 47 (2006) 1490.
[13] A.R. Korsgaard, R. Refshauge, M.P. Nielsen, M. Bang, S.K. Kaer, J. Power Sources 162 (2006) 239.
[14] G. Lin, W. He, T.V. Nguyen, J. Electrochem. Soc. 151 (2004) A1599.
[15] C.P. Wang, H.S. Chu, J. Power Sources 159 (2006) 1025.
[16] T.E. Springer, T. Rockward, T.A. Zawodzinski, S. Gottesfeld, J. Electrochem. Soc. A11 (2001) 148.
[17] H.S. Chu, C.P. Wang, W.C. Liao, W.M. Yan, J. Power Sources 159 (2006) 1071.